Seventh International Conference on Control, Automation, Robotics And Vision (ICARCV'02), Dec 2002, Singapore

FINITE ELEMENT TORQUE MODELING FOR THE DESIGN OF A SPHERICAL MOTOR

Raye A. Sosseh
Seagate Technologies
Servo Engineering Technology
Oklahoma City, OK 73134

Kok-Meng Lee
Georgia Institute of Technology
The George W. Woodruff School of Mechanical Eng.
Atlanta, GA 39332-0405

ABSTRACT

This paper presents the method of modeling the torque generated by a variable reluctance spherical motor (VRSM) that presents some attractive possibilities by combining pitch, roll, and yaw motion in a single joint. Unlike prior works on the torque formulation of a VRSM, which were based on a lumped-parameter approach using equivalent magnetic circuits (widely used in developing force/torque models for electromechanical devices), this paper presents a distributed-parameter approach to predict the motor's magnetic field distribution for formulating the torque of a VRSM. A detailed three-dimensional finite-element (FE) analysis has been performed on a VRSM configuration that consists of both permanent magnet (PM) poles and air-cored electromagnets. The model obtained using FE methods offers more insight and an accurate representation of torque generated by a spherical motor.

1. INTRODUCTION

The rapid advancement of robotics in the 1980's has motivated the development of several types of multiple-DOF actuators. Among these are the ball-joint-like spherical motors. The dominant types of spherical motors independently developed in the late 1980's are the induction type, the variable reluctance motor that includes the stepper, and the direct current motor. As compared with its counterpart, the VR spherical motor has a relatively large range of motion, possesses isotropic properties in motion, and is relatively simple and compact in design. The trade-off, however, is that sophisticated torque modeling for the design and control of a VRSM is required.

A number of research efforts at Georgia Tech have contributed to the development of torque model for a multi-DOF spherical motor. Lee *et al.* [1] presented the dynamic model of a VR spherical motor, which included the development of a torque model of the spherical motor in a quadratic form. The torque model describes the electromagnetic interaction of the spherical motor and defines the actuating torques for a specified set of electrical inputs to the stator coils at any given rotor orientation. The lumped-parameter torque model is developed using equivalent magnetic circuits, where permeance models play an important role in predicting the torque generated by the motor. The permeance model was first studied conceptually by Lee and Kwan [2] using assumed flux paths, and was further investigated theoretically by Lee *et al.* [3] using finite-element methods, and experimentally by Lee *et al.* [1]. Pei [4] used both the two-dimensional (2D) vector potential and 3D reduced scalar potential formulations to analyze the magnetic flux paths. While the 2D formulation offers a better visualization of the flux paths, a 3D analysis can provide a more accurate account of the magnetic field distribution. However, Pei's work [4] stopped short at modeling the permeance (or the reciprocal of the magnetic reluctance) used in equivalent magnetic circuit models. Roth [5] developed an experimental method and algorithms to determine the permeance model. The results agreed well with the theoretical models proposed by Lee and Kwan [2] and Lee *et al.* [3]. To reduce the contact reaction between the rotor and stator, Zhou and Lee [6] extended the torque model from three degrees-of-freedom (DOF) to six-DOF and also derived a maximum torque formula to characterize the spherical motor's output torque capability. The motor designs to date have been based on arguments employing magnetic circuit concepts. The ability to accurately model the torque and predict the torque for a given design geometry is essential for high precision motion control applications.

The spherical motor referred to in this paper has a similar structure as the ball-joint-like device [1]. Unlike prior works on the torque formulation of a VR spherical motor, which were based on a lumped-parameter approach using equivalent magnetic circuits (widely used in developing force/torque models for electromechanical devices), this paper uses a distributed-parameter approach to predict the motor's magnetic field distribution for formulating the torque of a spherical motor. Torque models developed using the solution to the spherical motor's magnetic field distribution give better insight and a more accurate formulation of the spherical motor torque. The field distribution in a typical electromechanical device like the spherical motor is governed by a set of partial differential equations commonly referred to as Maxwell's equations. Closed-form solutions to these equations are rather cumbersome and are only available for a few devices with relatively simple structures. In this paper, Maxwell's equations that govern the spherical motor field distribution are formulated using scalar potential functions and solved using FE methods. The FE package, ANSYS, written by Swanson [7] has been used to predict the magnetic fields [8].

The remainder of this paper is organized as follows: Section 2 presents the governing equations for calculating the force/torque generated by the spherical motor from the magnetic field distribution. Sections 3 and 4 provide an in-depth analysis of the magnetic field and torque generated by the interaction between a pair of electromagnetic coils and a pair of permanent magnet rotor poles, a basic torque generating unit. The application of the solution obtained using the FE analysis to a

specific VRSM design configuration is presented in Section 5. The conclusions are made in Section 6.

2. GOVERNING EQUATIONS

The torque of an electro-magnetic actuator is a function of magnetic field distribution governed by Maxwell's equations:

$$\nabla \bullet \mathbf{B} = 0 \tag{1}$$

$$\nabla \times \mathbf{H} = \mathbf{J} \tag{2}$$

where $\mathbf{B}$ is the magnetic flux density; $\mathbf{H} = \mathbf{H}_s + \mathbf{H}_m$ is the magnetic field intensity; and $\mathbf{J}$ is the current density. The magnetic field intensity due to the current source $\mathbf{H}_s$ is solved using the Biot-Savart law:

$$\mathbf{H}_s = \frac{1}{4\pi} \int_V \frac{\mathbf{J} \times \mathbf{r}}{|\mathbf{r}|^3} dV \tag{3}$$

where $\mathbf{r}$ is the position vector from the current source to a node and V is the volume of the current source. The magnetization of the material $\mathbf{H}_m$ is curl free and expressed in terms of a scalar potential function Φ :

$$\mathbf{H}_m = -\nabla \Phi \tag{4}$$

Using the constitutive relationship

$$\mathbf{B} = \mu \mathbf{H} \tag{5}$$

and Equation (4), Equation (1) can be written as

$$\nabla \bullet (\mu \nabla \Phi) = 0 \tag{6}$$

This is commonly referred to as Laplace's equation.

The solutions to the Laplace equations in regions of different materials require a set of boundary conditions. The following conditions at the interface boundary between any two regions with different material properties must be satisfied.

$$\mathbf{n}_{kj} \times (\mathbf{H}_j - \mathbf{H}_k) = \mathbf{J}_s \tag{7a}$$

$$\mathbf{n}_{kj} \bullet (\mathbf{B}_j - \mathbf{B}_k) = 0 \tag{7b}$$

where $\mathbf{n}_{kj}$ is a unit vector perpendicular to the surface boundary directed from the k^{th} medium to the j^{th} medium; and $\mathbf{J}_s$ is the surface current density at the interface.

Once the magnetic field distribution is solved with an appropriate set of boundary conditions, the torque generated by the spherical motor can be computed using Equation (8:

$$\mathbf{T} = -\int_V \mathbf{a} \times (\mathbf{J} \times \mathbf{B}) dV \tag{8}$$

where $(\mathbf{J} \times \mathbf{B})$ is the Lorentz force; and $\mathbf{a}$ represents the moment arm perpendicular to the axis of rotation and directed to the point at which the force is computed.

The magnetic field distribution is required to evaluate the generated torque. The challenge for solving the Laplace's equation for the magnetic field distribution of a spherical motor is due to the boundary conditions that result from the complex spherical motor arrangement of the rotor poles and the inherent 3-D nature of the problem. For this reason, the Laplace equation is solved numerically using FE methods for the magnetic scalar potential from ANSYS. The magnetic field intensity and flux density are then derived from the potential functions. Since the ANSYS FE package does not provide torque as an output, a macro was written to compute the generated torque by summing the cross products of the elemental force with its centroid using Equation (8).

3. 3D FE ANALYSIS OF THE MAGNETIC FIELDS

Figure 1 shows a typical relationship between a pair of rotor poles and a pair of stator coils that make up the basic torque generating unit, where the rotor caps and base are made up of high permeability iron. In formulating the magnetic field distribution of the spherical motor, the space occupied by the motor is divided into five regions. As shown in Figure 1, Region 1 is the free space (air). The permanent magnets of the rotor pole occupy Region 2. The iron cap and base for the rotor pole make up Regions 3 and 4 respectively. Region 5 defines the stator coil. For free space regions; a relative permeability of $\mu_r = 1$ is specified. For iron regions, the material properties can be specified in terms of either relative permeability or a *BH* curve. For PM regions, the required material properties are components of the magnetic coercive force vector and the PM relative permeability. The coercive force vector components specify the magnetization axis of the PM. The relative permeability of the PM is expressed as

$$\mu_{rm} = \frac{B_r}{\mu_o H_c} \tag{9}$$

where B_r is the residual magnetization; and H_c is the magnitude of the coercive force vector.

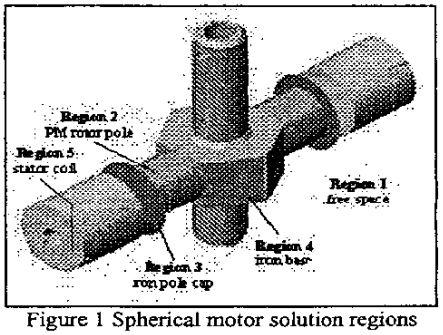

Figure 1 Spherical motor solution regions

The specific ANSYS program uses SOLID96 elements to mesh the rotor structure shown in Figure 1. The electromagnets are modeled by SOURCE36 elements. The FE model is completed by enclosing the rotor and stator coils with a volume of air (or free space) and by modeling the free space boundary with far field boundary using INFIN47 elements.

An ANSYS program is written to predict the magnetic field distribution between a pair of stator coils and rotor poles with a separation angle of 30° as shown in Figure 2. For the computation, a relative permeability of $\mu_r = 1$ and $\mu_r = 1000$ is used for the free space and iron regions respectively. For the PM regions, a magnetic coercive force magnitude of $H_c = 795{,}770\ A/m$ and a residual magnetization of $B_r = 1.12T$ are used. The coil geometry is given in Table 1.

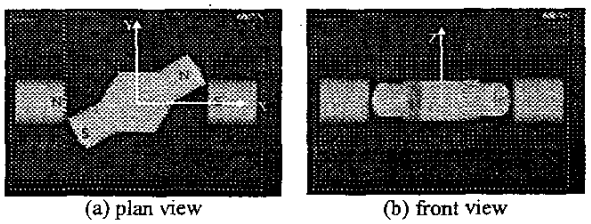

(a) plan view (b) front view

Figure 2 Interaction between stator coil and rotor pole

Table 1 Stator Coil Geometry

GEOMETRY	VALUES
Coil amperes-turns	4A, 1000 turns
Inside and outside radii	4.76 mm, 12.7mm
Length	25.4 mm
Rotor/stator air gap	0.762 mm

Figure 3 shows the distribution of the magnetic scalar potential obtained from the finite element solution. The increase in potential from left to right implies that the magnetic flux density vector is directed right. This results since the flux density points from the South Pole to the North Pole. Using Equation (4) and the constitutive relation in Equation (5), ANSYS computes the magnetic field intensity and flux density for each region in the spherical motor workspace. Figures 4(a) and 4(b) show detailed plots of the scalar potential and flux density distribution in the rotor region. The iron caps of the rotor poles are at a constant potential. Due to the symmetry of the location of the poles and the equal and opposite excitation of the stator coils, the magnetic scalar potential of the rotor base is almost zero.

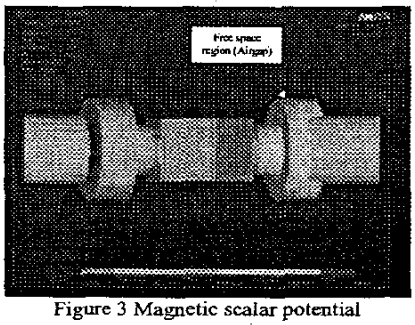

Figure 3 Magnetic scalar potential

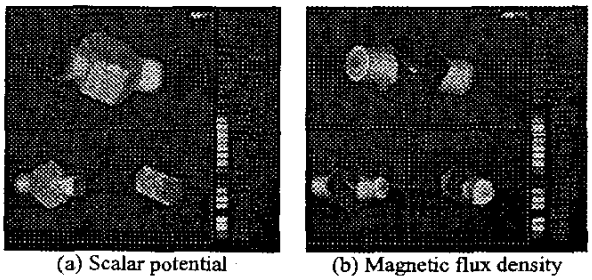

(a) Scalar potential (b) Magnetic flux density

Figure 4 Field distribution in the rotor

The magnetic flux density distribution in the free space (air) region is essential for evaluating the torque of the spherical motor. Figures 5(a) and 5(b) show the magnetic scalar potential and flux distribution in the free space region. The magnetic flux density is uniform immediately around the rotor pole cap and is aligned with the pole's magnetization axis.

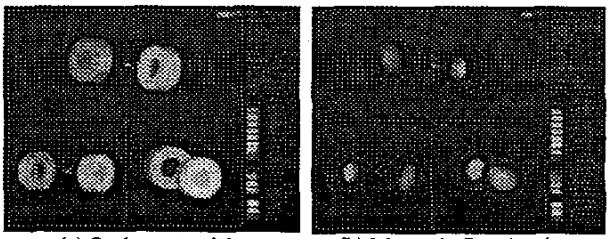

(a) Scalar potential (b) Magnetic flux density

Figure 5 Field distribution in the air space

4. 3D FE ANALYSIS OF THE MOTOR TORQUE

The uniform magnetic field density over the stator coil suggests that the torque in Equation (8) may be computed from the cross product of the stator coil's dipole moment $\mathbf{m}$ and the flux density due to the rotor pole.

$$\mathbf{T} = \mathbf{m} \times \mathbf{B} \tag{9}$$

For cylindrical stator coils, the magnetic dipole moment is

$$\mathbf{m}_j = \frac{n_c i_j}{L_c} A \bar{e}_{sj} \tag{10}$$

where $\bar{e}_{sj}$ is the orientation vector of the j^{th} stator coil; n_c is the number of turns in the coil; L_c is the length of the electromagnet; and A is the mean surface area of the coil.

4.1 Torque-current relationship

The torque generated by the interaction between the stator coils and rotor poles, similar to that shown in Figure 2 but with a separation angle of 16°, is computed using the ANSYS program as a function of stator coil current varied from –4A to 4A in increments of 0.5A. The computed torque is displayed in Figure 6.

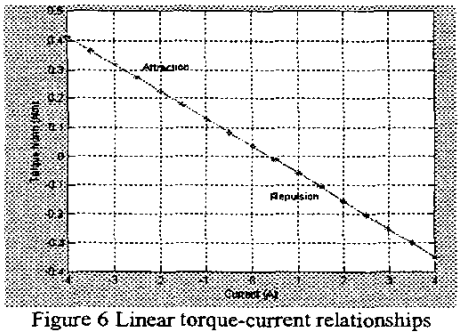

Figure 6 Linear torque-current relationships

In Figure 6, the change in sign of the z component of the torque indicates the switch from repulsion to attraction of the spherical motor rotor. The finite element results in Figure 6 show a linear relationship between the spherical motor torque

and the stator coil current input. This linear relationship implies that the contribution of self and mutual inductances on the torque is small compared to that contributed by the interaction between the air-cored electromagnets and the PM rotor poles.

4.2 Torque direction

The linear toque-current relationship and that the magnetic flux density is aligned with the pole's magnetization axis further suggest that the torque generated by the pair of stator coils and rotor poles has the following form:

$$\mathbf{T}_{jk} = f(\varphi_{jk}) \frac{\mathbf{S}_j \times \mathbf{R}_k}{|\mathbf{S}_j \times \mathbf{R}_k|} n_c i_j \qquad (11)$$

where $\mathbf{R}_k$ is the unit vector describing the locations of the k^{th} rotor pole in stator-fixed frame; and $f(\varphi_{jk})$ is an even function of the rotor orientation for a given geometry of electromagnets and rotor poles.

Table 2 summarizes the torque integrated using Equation (8) with the magnetic field obtained from the ANSYS computation for two different orientations of the rotor pole-pair with respect to the pair of stator coils. Table 2 also shows that the direction of the torque computed from the cross product of the unit vectors describing the stator-coil and the rotor-pole magnetization axes closely agree with the theoretical predictions of Equations (8), (9) and (10).

Table 2: Torque Direction

Coil Orientation - $\mathbf{S}_j$	[-.309, -.951, .000]	
Pole Magnetization Axis - $\mathbf{R}_k$	[.500, .866, .000]	[.179, .970, .163]
Torque (ANSYS) T (Nm)	[.015, -.009, -.305]	[.285, -.092, .228]
Torque Direction, $T/\lvert T\rvert$	[.049, -.029, -.998]	[.754, -.245, .609]
$-(\mathbf{S}_j \times \mathbf{R}_k)/\lvert \mathbf{S}_j \times \mathbf{R}_k \rvert$	[.000, .000, -1.00]	[.745, -.242, .622]

4.3 Torque characteristic function

In addition, both of these two rotor orientations in Table 2 have the same separation angle (or the angle between the coil axis and the magnetization axis of the rotor PM) of 12°. The magnitude of the resultant torque generated for the orientations #1 and #2 are 0.306Nm and 0.376Nm respectively; they are within 0.07Nm of each other. This difference is within the error limits due to the finite element mesh. The result is expected since the rotor pole and the stator coil are axis-symmetric. For a given geometry, the magnitude of the torque generated by the coil/pole interaction (for the symmetric structure as shown in Figure 1) depends only on the separation angle between the rotor pole and the stator coil, φ_{jk}.

To determine the torque characteristic function, the magnitudes of the resultant torque were computed for separation angles ranging from –36° to 24° in 3° increments with the setup shown in Figure 2. The torque characteristic function computed as a function of separation angle

$$f(\varphi_{jk}) = \frac{\|T_{jk}\|}{n_c i_j} \qquad (12)$$

is shown in Figure 7.

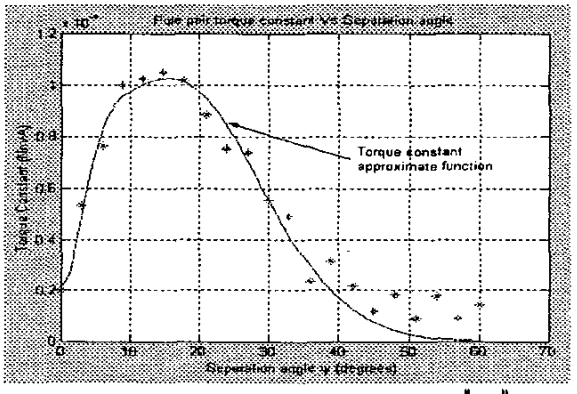

Figure 7: Torque characteristic function $f(\varphi_{jk}) = \|T_{jk}\| / n_c i_j$

The torque characteristic function in Equation (16) is approximated using a radial basis transfer function with the following form:

$$\hat{f}(\varphi_{jk}) = \sum_{n=1}^{N_f} \alpha_n \exp(-\lambda_n \varphi_{jk}^2) \qquad (13)$$

where the estimation coefficients α_n and λ_n and the order of the estimation function N_f are determined such that the norm squared of the estimation error $\|f(\varphi_{jk}) - \hat{f}(\varphi_{jk})\|^2$ is minimized. For the specific geometry shown in Figure 1 and Table 1, the coefficients for the approximate function are given in Table 3. Equations (12) and (13) are compared in Figure 7.

Table 3: Coefficients for $\hat{f}(\varphi_{jk})$ with $N_f = 4$

n	λ_n	α_n
1	8.02	-35.62
2	7.85	35.89
3	38.90	0.10
4	176.61	-0.28

5. TORQUE MODEL OF THE SPHERICAL MOTOR

Figure 8 shows the design example considered in this paper. The structure consists of N_r neodymium-iron-boron permanent magnets (PM) poles, and 2 layers of N_s stator coils.

The locations of the rotor poles and their magnetization axes ($\mathbf{r}_k$ and $\mathbf{M}_k$ for $k = 1, \cdots, N_r$ respectively) are represented by unit vectors in the rotor frame (xyz) as

$$\mathbf{r}_k = [C_{k\theta_r} \quad S_{k\theta_r} \quad 0]^T \qquad (14)$$

$$\mathbf{M}_k = (-1)^{(k+1)} \mathbf{r}_k \qquad (15)$$

where $C_{k\theta_r}$ and $S_{k\theta_r}$ denote the cosine and sine of the angle $k\theta_r$; θ_r is the angle between any two adjacent rotor poles.

Similarly, the location of the j^{th} stator coil on the l^{th} layer in stator-fixed frame (XYZ) is expressed as

$$\mathbf{S}_j = (-1)^{(l+1)} \left[C_{m\theta_s} C_{\alpha_s} \quad S_{m\theta_s} C_{\alpha_s} \quad S_{\alpha_s} \right]^T \qquad (16)$$

where $j = ml$; $l = 1,2$ denotes the layer; $m = 1, \cdots, N_s$ is the pole number on a given layer; θ_s is the angle between adjacent stator poles; and α_s is the inclination angle of stator coil layer from the XY plane. In order to have no generated torque when there are no current excitations, the stator coils are wound on non-ferromagnetic cores.

Typical Geometrical values for the design example are summarized in Table 4.

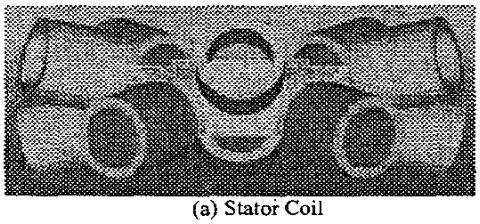

(a) Stator Coil

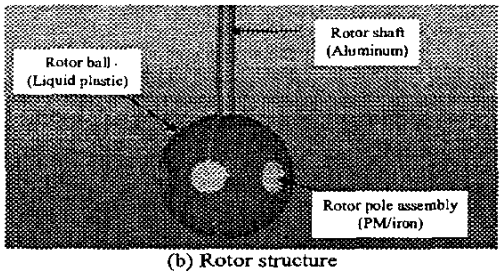

(b) Rotor structure

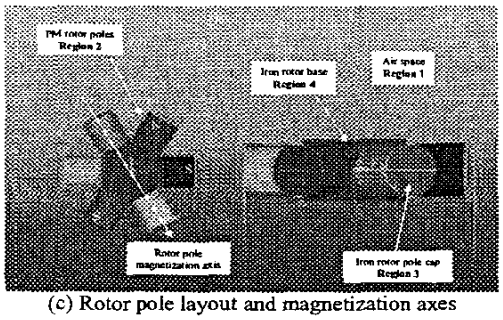

(c) Rotor pole layout and magnetization axes

Figure 8 Example solid model of a spherical motor

Table 4 Geometry of the design example

Parameters	Values
θ_s	72°
θ_r	60°
α_s	26.565°
Ns	10
Nr	6
Radius of the rotor	75mm

The results presented in Sections 3 and 4 have been computed for the interaction between a pair of rotor poles and a pair of air-cored electromagnets. If the principle of superposition holds, the torque model of the complete spherical motor can be derived from the model presented in Figure 1. In other words, the torque of the complete spherical motor can be deduced from the vector summation using Equations (11) and (13) for a specified coils and rotor poles.

The principle of superposition was verified by evaluating the torque that results from the interaction of one stator coil pair with two pairs of rotor poles, and comparing these results with the torque obtained by summing up results from individual pole pair interactions. Figure 9 shows the corresponding simulation results computed using the setup similar to that shown in Figure 2. The superposition of the two individual cases came very close to the case with the combined rotor poles. This verifies that the torque generated by the interaction of one stator pole pair with N rotor pairs is similar to summing up the interaction of N one pole-pair interactions. Therefore, the torque generated by the interaction of one stator pole pair and N rotor pole pairs can be evaluated as follow:

$$\hat{T}_{jN} = \sum_{k=1}^{N} \hat{f}(\varphi_{jk}) \frac{\mathbf{S}_j \times \mathbf{R}_k}{|\mathbf{S}_j \times \mathbf{R}_k|} n_c i_j \qquad (17)$$

The principles of superposition are finally validated if the torque generated by adding one more stator pair results in the same torque as the sum of the individual pair interactions. Similarly, the superposition of the individual results agreed closely with the combined results. The error between the two cases falls within the error range due to the quality of the mesh. With this in mind, the spherical motor torque model has the following form:

$$\hat{T} = \sum_{j=1}^{M} \hat{T}_{jM} = \sum_{j=1}^{M} \sum_{k=1}^{N} \hat{f}(\varphi_{jk}) \frac{\mathbf{S}_j \times \mathbf{R}_k}{|\mathbf{S}_j \times \mathbf{R}_k|} n_c i_j \qquad (18)$$

In a more compact form, Equation (18) can be expressed as:

$$T = [K_t] I_s \qquad (19)$$

where $[K_t]$ is the spherical motor torque constant and I_s is the vector of stator pole coil current inputs. The form of the torque model is very conducive for feedback control as a linear as opposed to a nonlinear constrained optimization is needed to compute the stator coil current input vector [9]. This linear relationship not only reduces the computational requirement of the controller, but also a wider range of controller techniques is available to choose from. The form of the torque was exploited in the design of the robust back stepping controller [10].

6. CONCLUSIONS

The method of modeling the torque generated by a VR spherical motor using the 3D finite element formulation has been presented. The model obtained using FE methods offers more insight and an accurate representation of torque generated by a spherical motor, which is essential for both design optimization and control of the spherical motor. The FE method presented here can potentially reduce the number of configurations that need to be built and tested as it provides capabilities for investigating the effects of key parameters on the

torque performance. The capabilities offered by the ANSYS finite element formulation of the spherical motor could, therefore, lead to a significant reduction in the design cycle time.

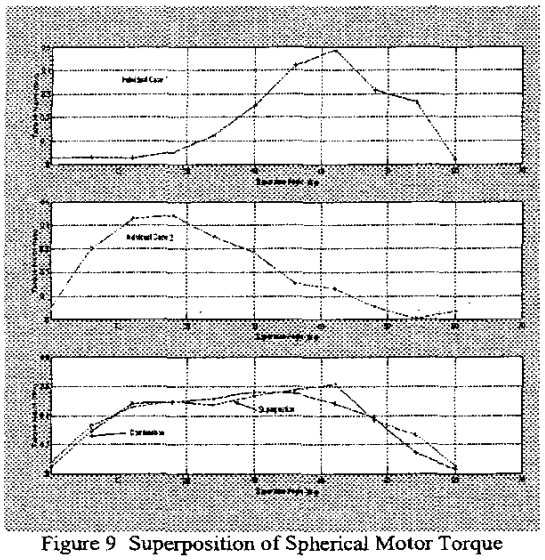

Figure 9 Superposition of Spherical Motor Torque

REFERENCES

[1] Lee, K-M., R. Roth, and Z. Zhou, "Dynamic Modeling and Control of a Ball-joint-like VR Spherical Motor," ASME *Journal of Dynamic Systems, Measurement and Control*, vol. 118, no. 1, pp. 29-40, March 1996.

[2] Lee, K-M. and C.-K. Kwan, "Design Concept Development of a Spherical Stepper for Robotic Applications," IEEE Trans. on Robotics and Automation, vol. 7, no.1, pp. 175-180, February 1, 1991.

[3] Lee, K-M., J. Pei and U. Gilboa, "On The Development Of A Spherical Wrist Actuator," Proc. of the 16th NSF Conf. on Manufacturing Systems Research, Tempe Arizona, January 8-12, 1990, pp. 295-301.

[4] Pei, J., "Methodology of Design and Analysis of a Variable Reluctance Spherical Motor," Ph.D. Thesis, Georgia Institute of Technology, December 1990.

[5] Roth, R., "An Experimental Investigation and Optimization of a Variable Reluctance Spherical Motor," Ph.D. Thesis, Georgia Institute of Technology, December 1992.

[6] Zhou, Z. and K-M. Lee, "Real-Time Motion Control of a Multi-Degree-of-Freedom Variable Reluctance Spherical Motor," Proc. of the 1996 IEEE ICRA, Minneapolis, MN, April 22-28, 1996, vol. 3, pp. 2859-2864.

[7] Seminar notes, "ANSYS: Magnetic Seminar," Swanson Analysis Systems, Inc., Houston, PA, 1987.

[8] Sylvester, P. and R. L. Ferrari, "Finite Elements for Electrical Engineers," Cambridge University Press, New York, 1986.

[9] Lee, K.-M. and R. Sosseh, "Effects of the Torque Model on the Control of a VR Spherical Motor," Proc. the 2nd IFAC Mechatronics, December 2002, San Francisco, CA.

[10] Lee, K.-M. and R. Sosseh, "Effects of the Fixture Dynamics on Back-stepping Control of a VR Spherical Motor," Proc. the 7th ICARCV 2002, December 3-6, Singapore.